Research Article

Qinhui Ren, Yufu Ma, Fuhua Wei*, Lan Qin, Hongliang Chen, Zhao Liang*, and Siyuan Wang

Preparation of Zr-MOFs for the adsorption of doxycycline hydrochloride from wastewater

https://doi.org/10.1515/gps-2022-8127 received October 10, 2022; accepted April 18, 2023

Abstract: Zr-metal-organic frameworks (Zr-MOFs) were prepared by a solvothermal method and characterized by X-ray diffraction, scanning electron microscopy, and thermogravimetry. Zr-MOFs were used to remove doxycycline hydrochloride (DOC) from wastewater. According to the experimental results, the maximum adsorption capacity of DOC by Zr-MOFs within 5 h was 148.7 $\rm mg\cdot g^{-1}$. From the pseudo-second-order kinetics model, all R^2 values were greater than 0.99, which proved that the adsorption of DOC by Zr-MOFs was consistent with practice. According to the Freundlich isotherm model, the adsorption of DOC by Zr-MOFs proceeded via multilayer adsorption. The aforementioned results show that Zr-MOFs have good application prospects for removing DOC from wastewater.

Keywords: MOFs, antibiotics, adsorption, wastewater treatment

1 Introduction

Antibiotics have been widely used in human and veterinary medicine to prevent and treat infectious diseases.

* Corresponding author: Fuhua Wei, College of Chemistry and

Chemical Engineering, Anshun University, Anshun, 561000,

Qinhui Ren, Yufu Ma, Lan Qin, Hongliang Chen: College of Chemistry and Chemical Engineering, Anshun University, Anshun, 561000, Guizhou, China

Siyuan Wang: State Key Laboratory of Advanced Design and Manufacturing for Vehicle Body, College of Mechanical and Vehicle Engineering, Hunan University, Changsha 410082, China However, due to poor metabolism in animals and humans. about 30-90% of administered antibiotics are excreted into the aquatic environment after treatment. Many antibiotics cannot be fully used and therefore enter nature, which may produce drug-resistant bacteria [1]. Doxycycline hydrochloride (DOC) readily dissolves in water [2]. Sewage treatment methods do not adequately remove antibiotics from water and sometimes produce secondary pollution. Therefore, many different technologies have emerged to remove DOC, including microbial degradation, phytoremediation, constructed wetland, microbial fuel cell enhanced biodegradation, constructed wetland-coupled microbial fuel cell degradation, and adsorption methods [3-6]. Among them, the degradation rate of the microbial degradation method and phytoremediation method is low. The constructed wetland method requires a large land area and long operation times. The enhanced biodegradation method of microbial fuel cells is restricted by many factors, such as solution concentration, electrode material, aeration rate, ionic strength, and external resistance and temperature, so the accuracy of the obtained data is low [7-9]. The removal rate using the constructed wetland-coupled microbial fuel cell degradation method is greatly affected by influent co-matrix and antibiotic concentration. Its development is also constrained by immature technology and high costs [10]. The adsorption method in this article has a simple procedure, is safe, uses simple equipment, has a narrow pH change, and uses less organic solvent to remove pollutants. However, it suffers from poor selectivity and unstable adsorbent performance.

Metal-organic frameworks (MOFs) have ultra-high specific surface areas, high and adjustable porosities, high adsorption capacities, easy synthesis and recycling [11], and show broad application prospects in many fields such as separation [12,13], energy storage [14,15], catalysis [16–22], adsorption [23–25], advanced oxidation [26], and devices [27–30]. Since MOFs have so many advantages, in this article, 2-amino-terephthalic acid was used as the organic chain and zirconium acetate as the metal ion to prepare Zr-MOFs, which were then used to remove DOC from an aqueous solution.

Guizhou, China, e-mail: wfh.1981@163.com

* Corresponding author: Zhao Liang, Institute of Micro/Nano
Materials and Devices, Ningbo University of Technology, Ningbo,
315211, China, e-mail: walleliang@163.com

2 Experimental

2.1 Experimental reagents and instruments

The ligand 2-amino-terephthalic acid, metal-derived zirconium acetate, and DOC were purchased from Shanghai Aladdin Biochemical Technology Co., Ltd.

An X-ray diffraction (XRD) diffractometer (Td-3300; Dandong Tongda Technology Co., Ltd.), a JSM-6700F field emission scanning electron microscope (Japan Electronics Co., Ltd.), an IRAffinity-1 infrared spectrometer, and a DTG-60 differential thermo resynchronization analyzer (Shimadzu, Japan) were used to analyze the Zr-MOFs. The structure and morphology of the materials were characterized.

2.2 Preparation of Zr-MOFs

The compound was synthesized according to the method previously described [16,20]. 2-Amino-terephthalic acid (0.3623 g) was dissolved in 15 mL of *N*,*N*-dimethylformamide (DMF). Then, 3.305 mL of zirconium acetate was mixed in a reaction kettle and then placed in a constant-temperature drying box set to 150°C. After reacting for 14 h, it was taken out and cooled to room temperature. The products were transferred to a centrifugal pipe and then centrifuged. Then, crystals were transferred to a beaker, magnetically stirred, and then washed three times with DMF and water. Centrifugation was repeated after each washing to remove unreacted starting matter, and the sample was put into a drying oven.

2.3 Removal of antibiotics by Zr-MOFs

Different masses of Zr-MOF samples obtained by the hot solvent method (20, 30, 40, and 50 mg) were added to 200 mL of DOC solutions with different concentrations (20, 30, 40, and 50 mg·L $^{-1}$). Then, they were stirred under natural light. Samples were taken every 30 min, and changes in antibiotic concentration in the solution at 269 nm were analyzed using a UV spectrometer. Then, by analyzing the relationship between time and concentration, the adsorption capacity and removal rate of DOC by Zr-MOFs were calculated. The adsorption capacity and removal rate of DOC were calculated using the following two formulas:

$$q_{\rm e} = \frac{(C_0 - C_{\rm e})V}{m} \tag{1}$$

Removal rate (%) =
$$\frac{(C_0 - C_t)}{C_0} \times 100\%$$
 (2)

where C_0 is the initial concentration of DOC, C_e is the concentration at adsorption equilibrium, C_t is the concentration at time t, V is the volume of solution, and m is the mass of Zr-MOFs.

3 Results and discussion

3.1 Structure of Zr-MOFs

The infrared spectrum in Figure 1 has strong absorption peaks at 1,581 and 1,375 cm⁻¹. Strong absorption peaks also appeared between 1,620–1,550 and 1,420–1,300 cm⁻¹, which indicate that carboxylic acids reacted with the metal salt [31,32]. In Figure 2, the XRD patterns of the materials show that Zr-MOF had a poor crystallinity and small particle size. Figure 3 shows that Zr-MOFs had a better morphology and dispersion. This was mainly because intermolecular interactions between organic ligands were weakened, and the deprotonation of organic ligands was enhanced, which promoted the growth of crystals in the solvent.

Figure 4 shows that the Brunauer–Emmett–Teller surface area was 405.7776 m²·g⁻¹. The adsorption average pore diameter was 3.61059 nm, indicating the mesoporous nature of the material. As can be seen from Figure 3, the Zr-MOFs displayed type IV of isotherms with H3 hysteresis loops, indicating the mesoporous properties of the sample.

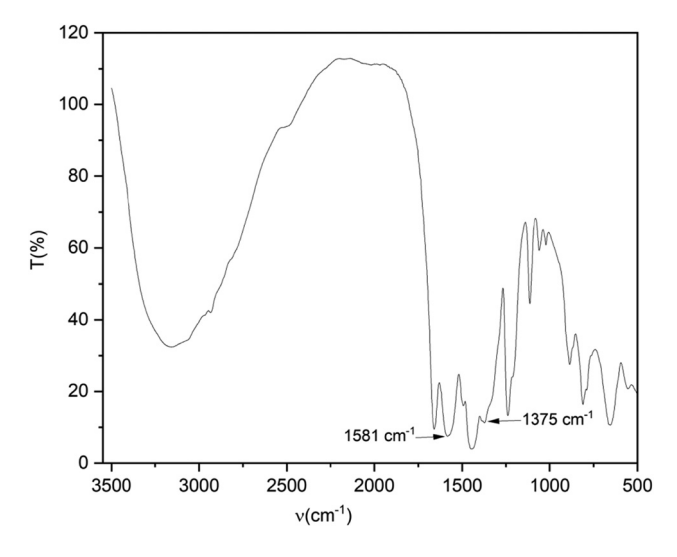


Figure 1: FTIR spectrum of Zr-MOF.

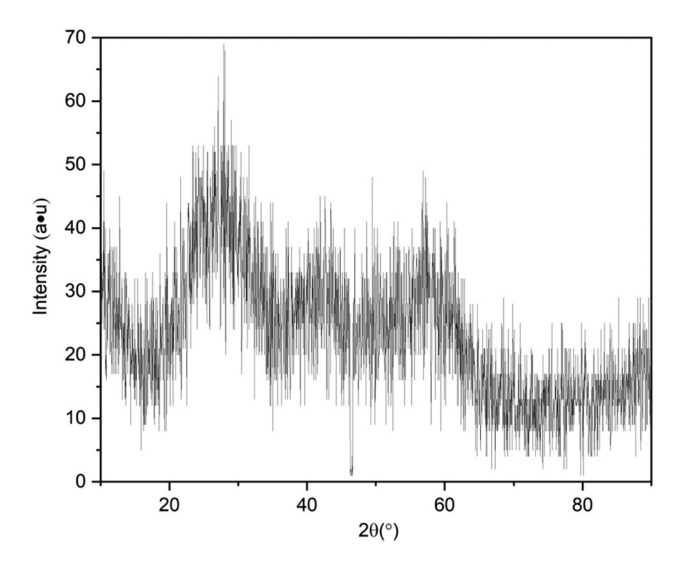


Figure 2: XRD pattern of Zr-MOF.

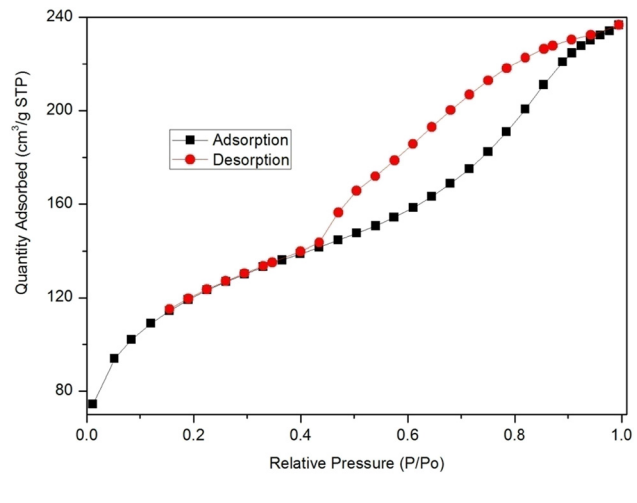
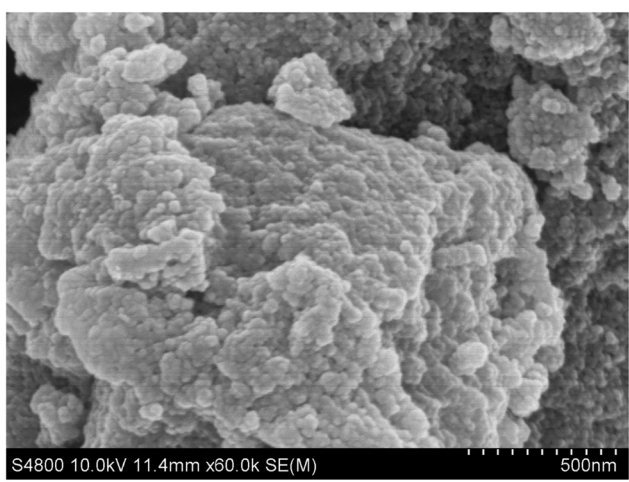


Figure 4: N₂ adsorption-desorption isotherms of Zr-MOF.



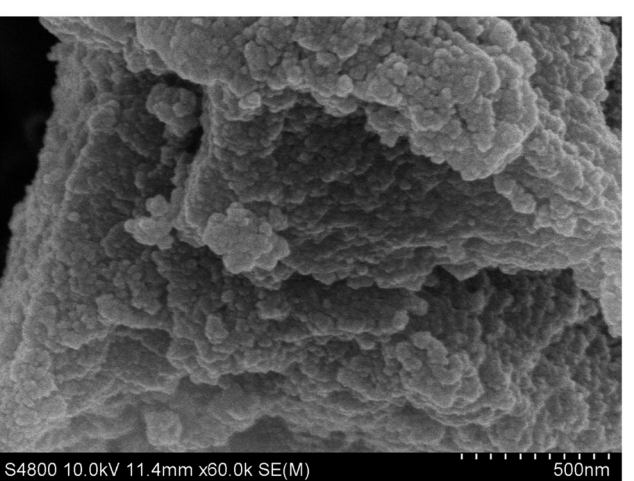


Figure 3: SEM images of Zr-MOF.

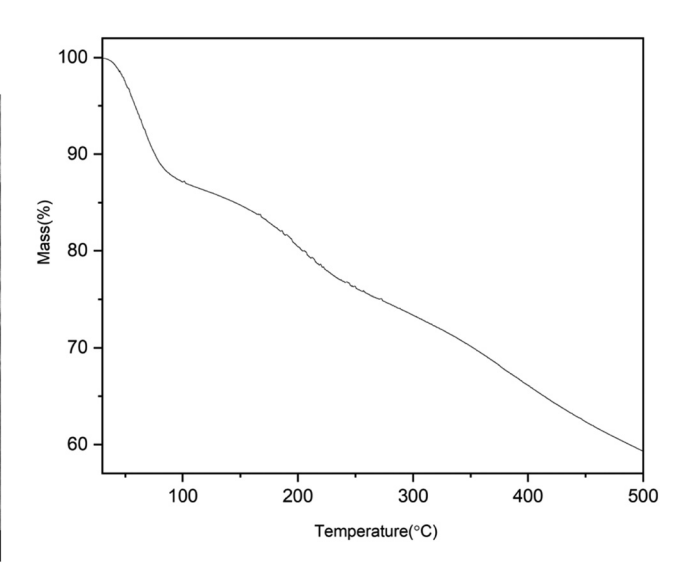


Figure 5: Thermogravimetric analysis of Zr-MOFs.

As shown in Figure 5, the thermogravimetric curves of the Zr-MOFs were characterized by three different stages: (1) a mass loss of 12.3% at about 90°C, which was dominated by residual solvent molecules; (2) a mass loss of 13% between 91°C and 275°C, which was mainly due to the oxidation of metal ions; and (3) a mass loss that began at 275°C and ended at 500°C, leaving a residual amount of 16% [33]. This corresponded to the destruction of the framework, indicating that the material was stable below 275°C. In most cases, Zr-MOFs generated via reactions between metal ions and organic ligands have more stable structures [34].

4 — Qinhui Ren et al. DE GRUYTER

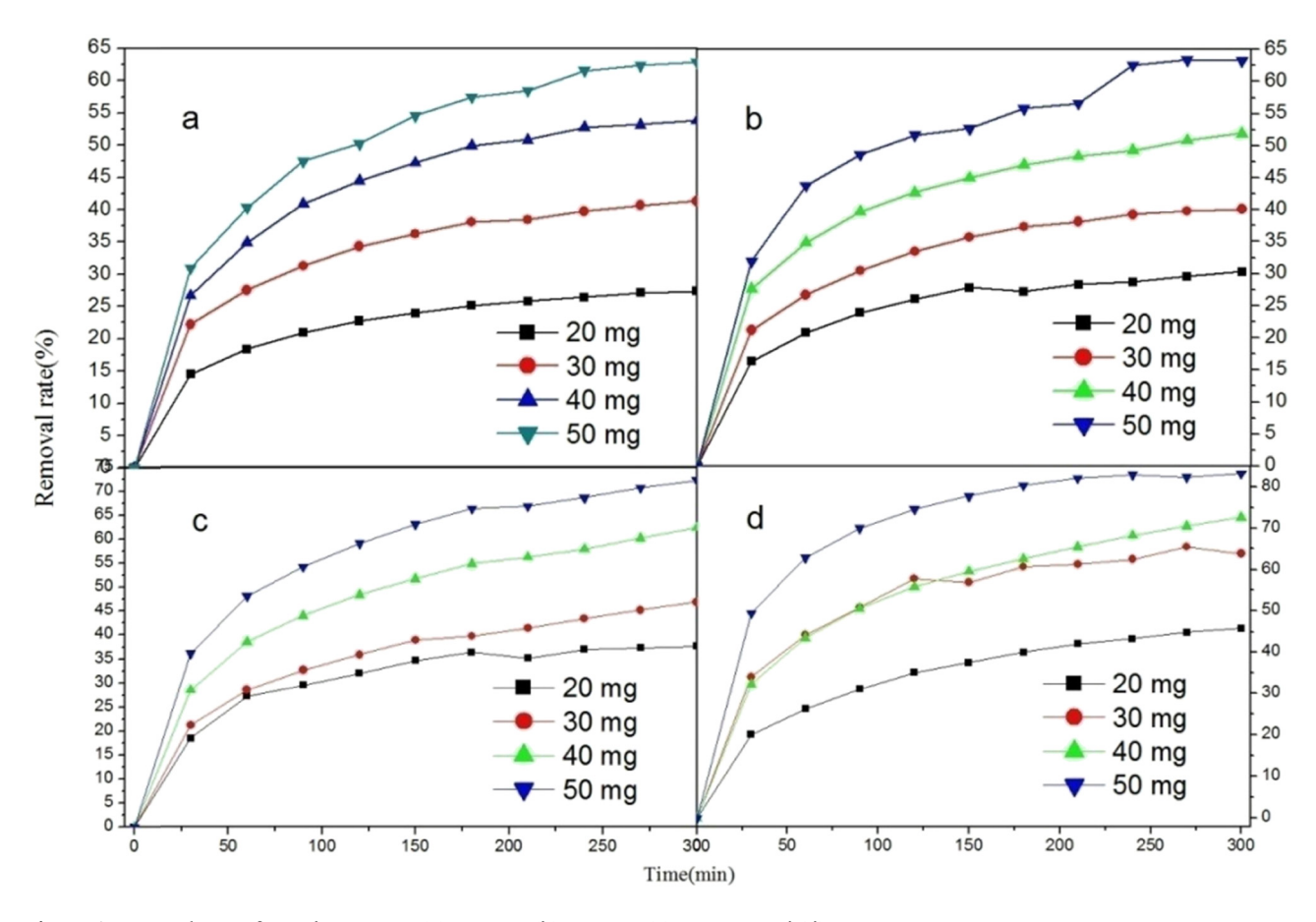


Figure 6: Removal rate of DOC by Zr-MOF: (a) 50 ppm, (b) 40 ppm, (c) 30 ppm, and (d) 20 ppm.

3.2 DOC removal using Zr-MOFs

To study the ability of Zr-MOFs to remove DOC, this experiment controlled the amount of Zr-MOFs, DOC-HCl, and reaction time. As shown in Figure 6, when the concentration of DOC was 30 ppm and the concentration of Zr-MOF was 50 mg, the removal rate reached 84.4% after 5 h. After three cycles, the removal rate of Zr-MOFs was 19.7%, indicating reasonable reusability (Figure 7). It can also be seen from the figure that when the concentration of DOC was unchanged, the removal rate gradually increased after adding Zr-MOF. When the dosage of Zr-MOF was constant, the removal rate increased upon decreasing the DOC concentration. When the mass of Zr-MOF was 30 mg, and the concentration of DOC was 50 mg·L⁻¹, the maximum adsorption capacity was 148.7 mg·g⁻¹.

To verify the consistency between theory and experimental practice, the first-order and second-order kinetics were simulated to study the removal of DOC by Zr-MOF. The results are shown in Figures 8 and 9 and Table 1. The formulas are as follows [35–37]:

$$ln\frac{C_t}{C_0} = k_1 t$$
(3)

$$\frac{t}{q_t} = \frac{t}{q_e} + \frac{1}{k_2 q_e^2} \tag{4}$$

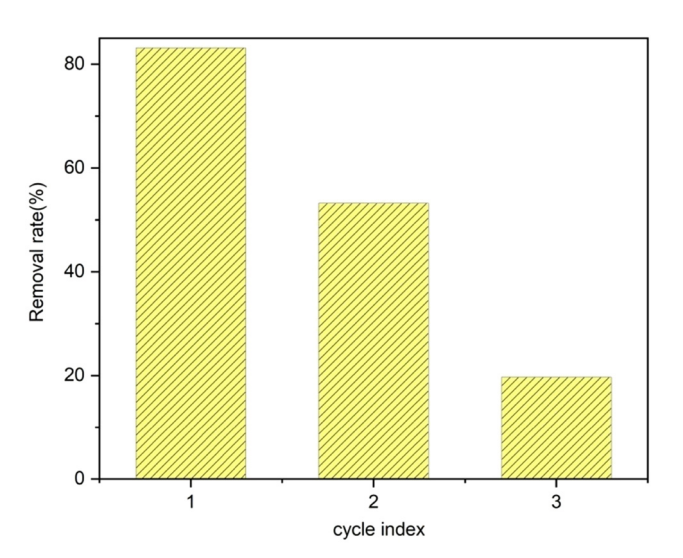


Figure 7: Reusability of Zr-MOFs for the removal of DOC.

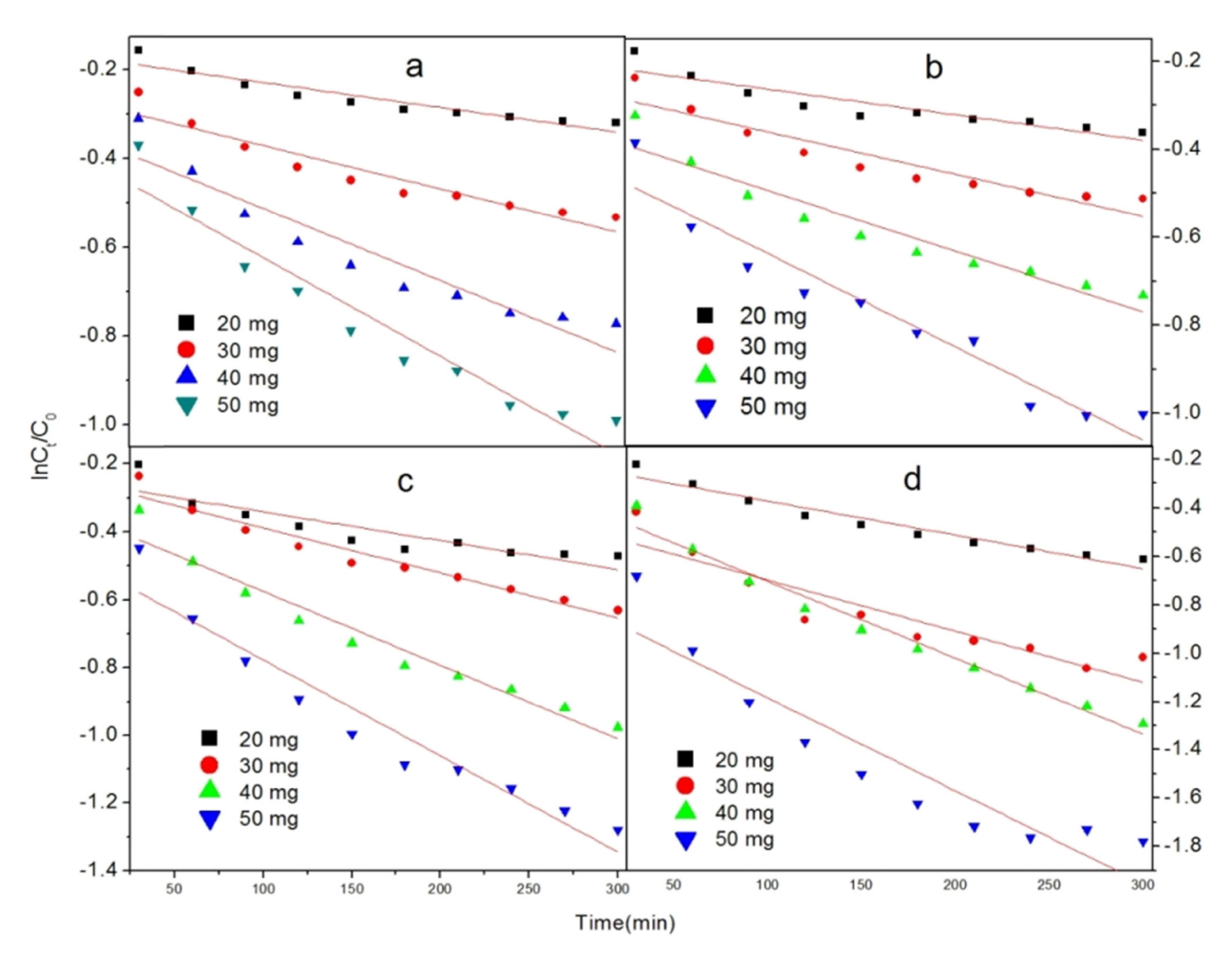


Figure 8: Pseudo-first-order kinetic model for the adsorption DOC over Zr-MOF: (a) 50 ppm, (b) 40 ppm, (c) 30 ppm, and (d) 20 ppm.

As shown in Figures 8 and 9 and Table 1, the R^2 value of the second-order kinetics model was better than that of the first-order model. The simulation results were in agreement with the experimental results. The adsorption of DOC by Zr-MOFs occurred mainly via chemisorption.

The experimental results were also analyzed by the Langmuir and Freundlich isotherm models [38,39]. When the concentration of DOC adsorbed by Zr-MOFs was 20 ppm, the parameters obtained by Langmuir and Freundlich models are shown in Figure 10 and Table 2. The R^2 values were 0.99162 and 0.99787, respectively. The data showed that the Freundlich model was more consistent with the experimental adsorption data of DOC, indicating that the adsorption of DOC by Zr-MOFs proceeded via multilayer adsorption.

To explore the effect of pH on DOC adsorption, 30 mg of Zr-MOF was added to 50 ppm DOC solutions with different pH values. As shown in Figure 11, the adsorption

capacity of DOC increased with the pH. The zeta potential of Zr-MOFs was –9.98 mV, which might be attributed to the strong electrostatic interactions between DOC molecules and Zr-MOF adsorbent surfaces. The maximum adsorption capacity was obtained at pH 6 and 10.

To verify the influence of temperature, 30 mg of Zr-MOFs was added to 50 ppm DOC solutions at different temperatures and compared with ambient normal temperature. The adsorption capacity slightly decreased upon increasing the temperature, and the adsorption effect was the best at ambient temperature.

To gain further insight into the mechanism of DOC adsorption, the thermodynamic equilibrium constant (K_0) and Gibbs free energy change (ΔG^0), enthalpy change (ΔH^0), and entropy change (ΔS^0) were determined using the following equations:

$$K_0 = \frac{q_e}{c_o} \tag{5}$$

6 — Qinhui Ren et al. DE GRUYTER

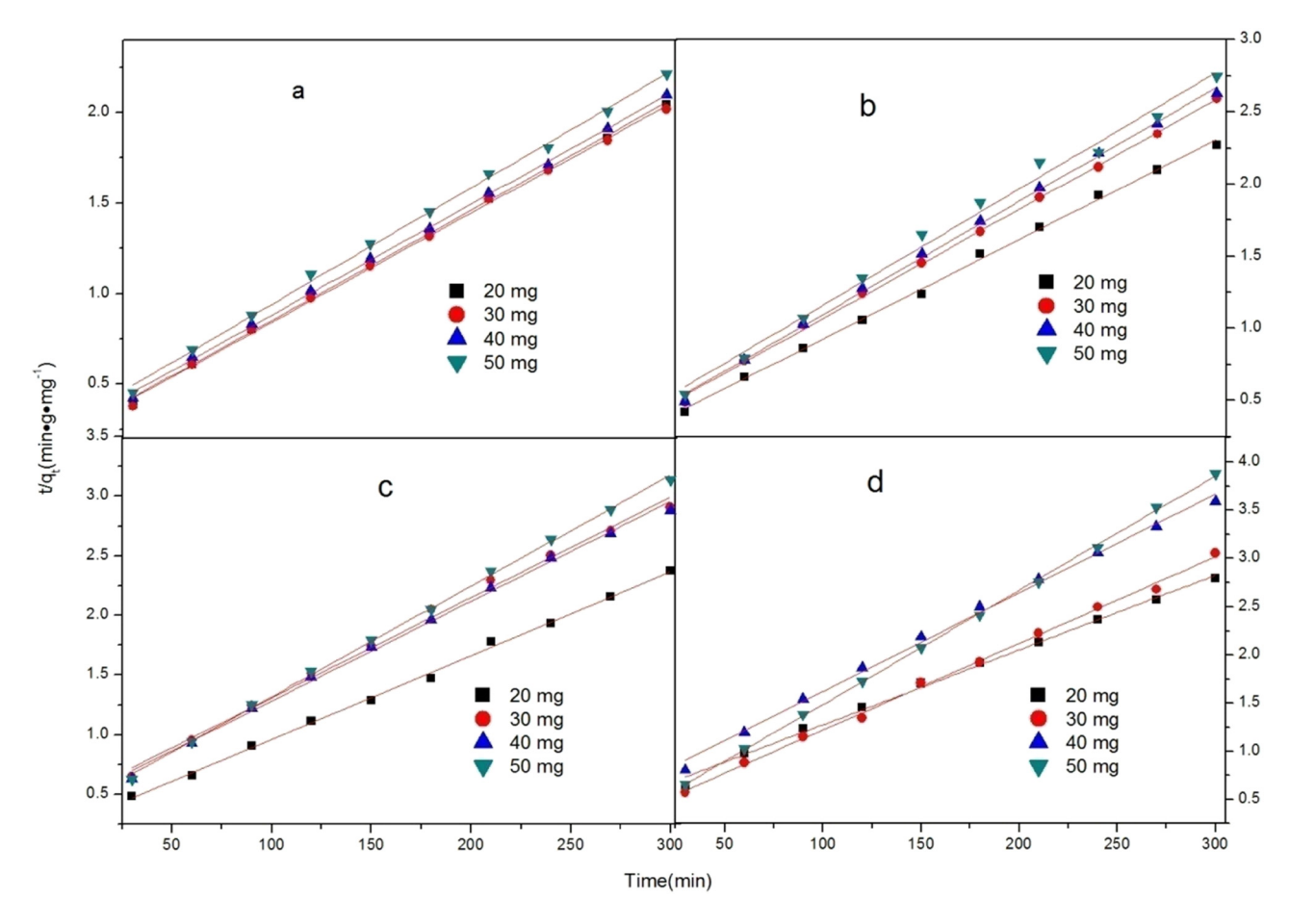
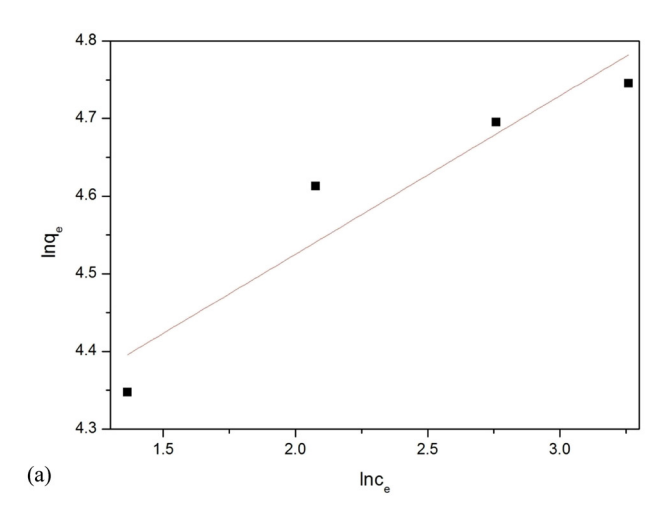


Figure 9: Pseudo-second-order (PSO) kinetic model for the adsorption DOC over Zr-MOF: (a) 50 ppm, (b) 40 ppm, (c) 30 ppm, and (d) 20 ppm.

Table 1: Kinetic parameters for the adsorption of DOC over Zr-MOF

Concentration	Mass	PSO kinetics		Pseudo-first-order kinetics	
		$K (g \cdot mg^{-1} \cdot min^{-1})$	R ²	K (L·min ⁻¹)	R ²
20	20	0.00776	0.9961	0.00139	0.94461
	30	0.00899	0.99768	0.00211	0.84618
	40	0.01023	0.99601	0.00317	0.97492
	50	0.01185	0.99949	0.00385	0.85806
30	20	0.00703	0.99804	0.0008454	0.78386
	30	0.00839	0.99436	0.00132	0.94285
	40	0.00835	0.99648	0.00218	0.95092
	50	0.00927	0.99878	0.00284	0.92905
40	20	0.00691	0.99818	0.0005822	0.82319
	30	0.00759	0.99889	0.009629	0.88152
	40	0.00786	0.99832	0.00139	0.9147
	50	0.00807	0.99164	0.00213	0.92649
50	20	0.00604	0.99884	0.0005586	0.88356
	30	0.00599	0.99838	0.0009758	0.89983
	40	0.00608	0.99922	0.00162	0.88962
	50	0.00638	0.99808	0.0022	0.92532



DE GRUYTER

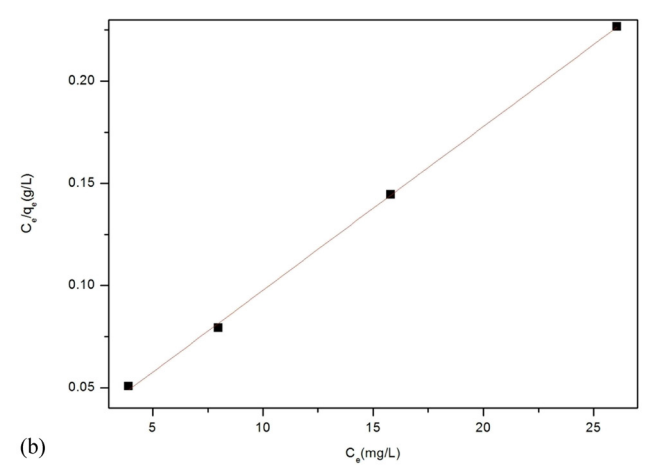


Figure 10: Adsorption isotherms of DOC adsorption onto Zr-MOFs:
(a) Freundlich isotherm and (b) Langmuir isotherm.

$$\ln K_0 = \frac{\Delta S^0}{R} - \frac{\Delta H^0}{RT} \tag{6}$$

$$\Delta G^0 = -RT \ln K_0 \tag{7}$$

where K_0 is the Langmuir adsorption constant (L·mol⁻¹) and R is the gas constant (8.314 J·mol⁻¹·K⁻¹). A linear plot of $\ln K_0$ versus 1/T was obtained as shown in Figure 8. ΔH^0 and ΔS^0 were calculated from (–slope × R) and (intercept × R) of the van't Hoff plot as shown in Figure 9 and Table 3.

As shown in Figure 12 and Table 3, the negative ΔG^0 and ΔH^0 values indicated that the adsorption of DOC over MOFs was spontaneous and exothermic. Enthalpy changes

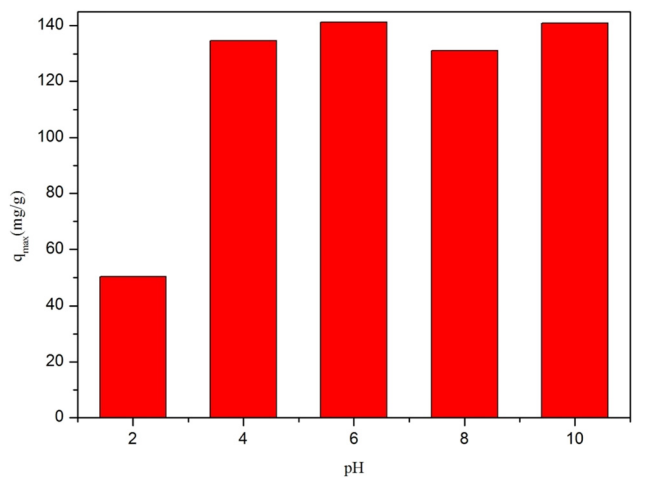


Figure 11: Effect of pH on the adsorption amount of DOC.

Table 3: Thermodynamic parameters of DOC adsorption onto MOFs

T (K)	ΔG^0 (kJ·mol ⁻¹)	ΔH^0 (-slope × R) (kJ·mol ⁻¹)	S^{o} (intercept $\times R$) ($J \cdot mol^{-1} \cdot K^{-1}$)
303	-10.5	-25.6	-49.7

due to chemisorption fall in the range of 84 and $420 \text{ kJ} \cdot \text{mol}^{-1}$, while physical absorption tends to occur below $84 \text{ kJ} \cdot \text{mol}^{-1}$ [40]. Thus, the adsorption of DOC over MOFs may have occurred by physisorption. Moreover, the entropy change ΔS^0 was positive, which revealed that the process increased the randomness because the number of desorbed water molecules was larger than that of adsorbed DOC molecules [41].

To study whether the removal of DOC by Zr-MOFs was affected by light, 30 mg of Zr-MOFs was added to 50 ppm DOC, and the results were compared under natural lighting and catalysis by a xenon lamp, as shown in Figure 13. After comparison and sampling within the same time period, the amount of DOC adsorbed under xenon lamp irradiation was $34.5 \, \mathrm{mg \cdot g^{-1}}$ less than that under natural light.

A comparison of the adsorption capacity of DOC by other materials is shown in Table 4. Zr-MOF had the best adsorption capacity for DOC. The adsorption of DOC by

Table 2: Adsorption isotherm parameters of DOC onto MOFs at room temperature

T (K)	Langmuir isotherm		m	Freundlich isotherm		
	k	R ²	$q_{\rm m}~({\rm mg\cdot g^{-1}})$	$K_{f} (mg \cdot g^{-1} \cdot (L \cdot mg^{-1})^{1/n})$	n	R ²
293	0.00801	0.99932	124.8	61.3925	4.9017	0.85564

8 — Qinhui Ren et al. DE GRUYTER

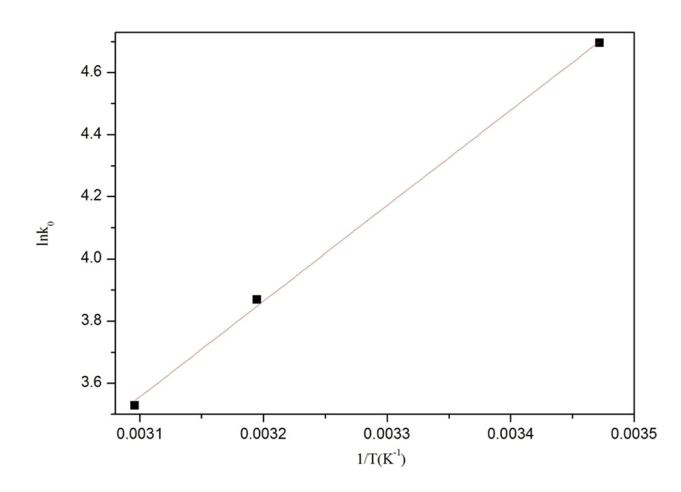


Figure 12: Van't Hoff plots used to determine the ΔH and ΔS of DOC adsorption over Zr-MOFs.

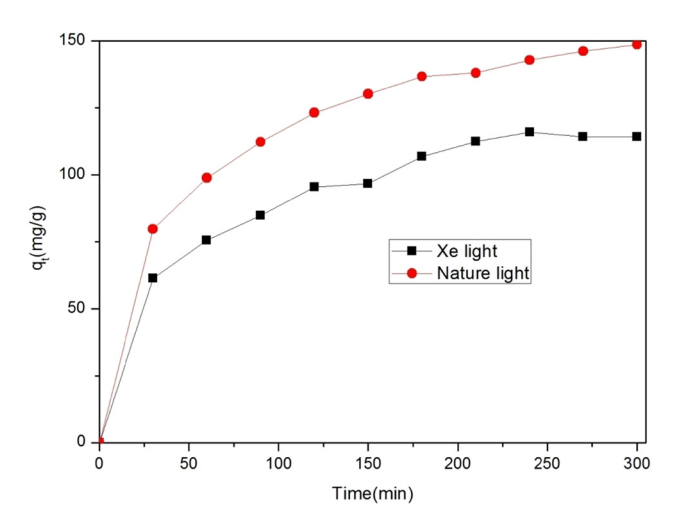


Figure 13: Comparison of DOC removal by Zr-MOFs.

Zr-MOFs occurred via a combination of chemisorption and physical adsorption, which led to a better removal effect. Zr-MOFs and DOC could form hydrogen bonds. Zr-MOFs are porous materials, which allow them to absorb DOC. Zr-MOFs may contain unreacted groups that could adsorb DOC via electrostatic adsorption. Because both Zr-MOFs and DOC have benzene rings, the two molecules

Table 4: Comparison of the adsorption capacity of different adsorbents for DOC removal

Adsorbents	$q_{max} \; (mg \cdot g^{-1})$	References
Zr-MOFs	148.7	This work
Graphene nanosheet	110	[42]
Cu(II)-impregnated biochar	93	[43]
Fe ₃ O ₄ magnetic nanoparticles	61.35	[44]
Electro-generated adsorbents	31.35	[45]

may be bound together by π – π stacking. Due to the aforementioned effects, Zr-MOFs could remove DOC [46–50].

4 Conclusion

A hot solvent method was used to prepare Zr-MOFs, which were characterized using XRD, scanning electron microscopy (SEM), Fourier-transform infrared spectroscopy (FTIR), and differential thermal-thermogravimetric analysis. Zr-MOFs were used to remove the antibiotic DOC, and the results showed that the best removal effect was with pH = 6 and pH = 10; simulated kinetics showed that DOC removal by Zr-MOFs followed the second-order kinetics model, with an $R^2 > 0.99$. The Langmuir and Freundlich isotherm model analysis showed that the adsorption mechanism was consistent with multilayer adsorption. It can be seen that DOC can be removed by Zr-MOFs and may have practical applications.

Funding information: This work was supported by Doctoral Fund of Anshun University (asxybsjj202103), Guizhou Education Department Youth Science and Technology Talents Growth Project (KY[2019]149), and Undergraduate Innovation and Entrepreneurship Project number [S202210667150].

Author contributions: Qinhui Ren writing – original draft; Fuhua Wei: writing – review and editing; Yufu Ma: methodology; Lan Qin, Hongliang Chen: formal analysis; Zhao Liang, Siyuan Wang: visualization.

Conflict of interest: The authors state no conflict of interest.

Data availability statement: The datasets generated during and analyzed during the current study are available from the corresponding author on reasonable request.

References

- [1] Cao B, Yu XL, Wang C, Lu S, Xing D, Hu X. Rational collaborative ablation of bacterial biofilms ignited by physical cavitation and concurrent deep antibiotic release. Biomaterials. 2020;262:120341.
- [2] Verma SK, Jha E, Panda PK, Thirumurugan A, Patro S, Parashar SKS, et al. Molecular insights to alkaline based biofabrication of silver nanoparticles for inverse cytotoxicity and enhanced antibacterial activity. Mat Sci Eng C-Mater. 2018;92:807–18.

- [3] Liu SG, Ding YQ, Li PF, Diao KS, Tan XC, Lei FH, et al. Adsorption of the anionic dye Congo red from aqueous solution onto natural zeolites modified with N, N-dimethyl dehydroabietylamine oxide. Chem Eng J. 2014;248:135–44.
- [4] Chen F, Yang Q, Li X, Zeng G, Wang D, Niu C, et al. Hierarchical assembly of graphene-bridged Ag₃PO₄/Ag/BiVO₄ (040) Z-scheme photocatalyst: An efficient, sustainable and heterogeneous catalyst with enhanced visible-light photoactivity towards tetracycline degradation under visible light irradiation. Appl Catal B. 2017;200:330-42.
- [5] Saleha TA, Sarıb A, Tuzen M. Optimization of parameters with experimental design for the adsorption of mercury using polyethylenimine modified-activated carbon. J Env Chem Eng. 2017:5:1079–88.
- [6] Hernández-Montoya V, Pérez-Cruz MA, Mendoza-Castillo DI, Moreno-Virgen MR, Bonilla-Petriciolet A. Competitive adsorption of dyes and heavy metals on zeolitic structures. J Env Manage. 2013;116:213–21.
- [7] Wang H, Yuan X, Wu Y. Synthesis and applications of novel graphitic carbon nitride/metal-organic frameworks mesoporous photocatalyst for dyes removal. Appl Catal B-Environ. 2015;174–175:445–54.
- [8] Huo SH, Yan XP. Metal-organic framework MIL-100(Fe) for the adsorption of malachite green from aqueous solution. J Mater Chem. 2012;22:7449-55.
- [9] Dias EM, Petit JC. Towards the use of metal-organic frameworks for water reuse: a review of the recent advances in the field of organic pollutants removal and degradation and the next steps in the field. Mater Chem A. 2015;3:22484-506.
- [10] Bajpai VK, Shukla S, Khan I, Kang SM, Haldorai Y, Tripathi KM, et al. A sustainable graphene aerogel capable of the adsorptive elimination of biogenic amines and bacteria from soy sauce and highly efficient cell proliferation. ACS Appl Mater Inter. 2019;11:43949-63.
- [11] Wei FH, Xiao L, Ren QH, Wang K, Qin L, Chen HL, et al. The application of Bimetallic metal-organic frameworks for anti-biotics adsorption. J Saudi Chem Soc. 2022;26:101562.
- [12] Jaramillo DE, Reed DA, Jiang HZH, Oktawiec J, Mara MW, Forse AC, et al. Selective nitrogen adsorption via backbonding in a metal-organic framework with exposed vanadium sites. Nat Mater. 2020;19(5):517–21.
- [13] Zhang L, Jee S, Park J, Jung M, Wallacher D, Franz A, et al. Exploiting dynamic opening of aperturesin partially fluorinated MOF for enhancing H-2 desorption temperature and isotope separation. J Am Chem Soc. 2019;141(50):19850-8.
- [14] Bi S, Banda H, Chen M, Niu L, Chen MY, Wu TZ, et al. Molecular understanding of charge storage and charging dynamics in supercapacitors with MOF electrodes and ionic liquid electrolytes. Nat Mater. 2020;19:552–8.
- [15] Boyd PG, Chidambaram A, Garcia-Diez E, Ireland CP, Daff TD, Bounds R, et al. Data-driven design of metal-organic frameworks for wet flue gas CO₂ capture. Nature. 2019;576(7786):253-6.
- [16] Bi FK, Zhao ZY, Yang Y, Liu Q, Huang WY, Huang YD, et al. Efficient degradation of toluene over ultra-low Pd supported on UiO-66 and its functional materials: Reaction mechanism, water-resistance, and influence of SO₂. Environ Funct Mater. 2022;1:166–81.
- [17] Zhang XD, Zhao ZY, Zhao SH, Xiang S, Gao WK, Wang L, et al. The promoting effect of alkali metal and $\rm H_2O$ on Mn-MOF

- derivatives for toluene oxidation: A combined experimental and theoretical investigation. J Catal. 2022;415:218-35.
- [18] Zhao SH, Yang Y, Bi FK, Chen YF, Wu MH, Zhang XD, et al. Oxygen vacancies in the catalyst: Efficient degradation of gaseous pollutants. Chem Eng J. 2023;454:140376.
- [19] Rao RZ, Ma ST, Gao B, Bi FK, Chen YF, Yang Y, et al. Recent advances of metal-organic framework-based and derivative materials in the heterogeneous catalytic removal of volatile organic compounds. J Colloid Interface Sci. 2023;636:55–72.
- [20] Jie BR, Lin HD, Zhai YX, Ye JY, Zhang DY, Xie YF, et al. Mechanism, design and application of fluorescent recognition based on metal organic frameworks in pollutant detection. Chem Eng J. 2023;454:139931.
- [21] Li HH, Yu JY, Gong YS, Lin NP, Yang QL, Zhang XD, et al. Perovskite catalysts with different dimensionalities for environmental and energy applications: A review. Sep Purif Technol. 2023;307:122716.
- [22] Yu JY, Li HH, Lin NP, Gong YS, Jiang H, Chen JJ, et al. Oxygendeficient engineering for perovskite oxides in the application of AOPs: Regulation, detection, and reduction mechanism. Catalysts. 2023;13(1):148.
- [23] Xiong G, Wang BB, You LX, Ren BY, He YK, Ding F, et al. Hypervalent silicon-based, anionic porous organic polymers with solid microsphere or hollow nanotube morphologies and exceptional capacity for selective adsorption of cationic dyes. Mater Chem. 2019;7(1):393–404.
- [24] Zhao QY, Zhao ZY, Rao RZ, Yang Y, Ling SY, Bi FK, et al. Universitetet iOslo-67 (UiO-67)/graphite oxide composites with high capacities of toluene: Synthesis strategy and adsorption mechanism insight. J Colloid Interface Sci. 2022;627:385-97.
- [25] Wang Y, Gong YS, Lin NP, Yu L, Du BB, Zhang XD. Enhanced removal of Cr(VI) from aqueous solution by stabilized nanoscale zero valent iron and copper bimetal intercalated montmorillonite. J Colloid Interface Sci. 2022;606:941–52.
- [26] Lin HD, Jie BR, Ye JY, Zhai YX, Luo ZJ, Shao GJ, et al. Recent advance of macroscopic metal-organic frameworks for water treatment: A review. Surf Interfaces. 2023;36:102564.
- [27] Ren QH, Nie M, Yang LL, Wei FH, Ding B, Chen HL, et al. Synthesis of MOFs for RhB adsorption from wastewater. Inorganics. 2022;10(3):27.
- [28] Li JN, Han X, Zhang XR, Sheveleva AM, Cheng YQ, Tuna F, et al. Capture of nitrogen dioxide and conversion to Nitric acid in a porous metal-organic framework. Nat Chem. 2019;11:1085–90.
- [29] Mohammad-Pour GS, Hatfield KO, Fairchild DC. A solid-solution approach for redox active metal-organic frameworks with tunable redox conductivity. J Am Chem Soc. 2019;141(51):19978–82.
- [30] Liang RR, Ru-Han A, Xu SQ, Qi QY, Zhao X. Fabricating organic nanotubes through selective disassembly of two-dimensional covalent organic frameworks. J Am Chem Soc. 2019;142:70-4.
- [31] Wei FH, Zheng T, Ren QH, Chen HL, Peng JH, Ma Y, et al. Preparation of metal-organic frameworks by microwave-assisted ball milling for the removal of CR from wastewater. Green Process Synth. 2022;11(1):595–603.
- [32] Ren QH, Wei FH, Chen HL, Chen D, Ding B. Preparation of Zn-MOFs by microwave-assisted ball milling for removal of tetracycline hydrochloride and Congo red from wastewater. Green Process Synth. 2021;10(1):125-33.

- [33] Crabtree RH. The organometallic chemistry of the transition metals. 5th edn. East China University of Science and Technology Publishing Co. Ltd.; 2012. p. 148.
- [34] Nguyen VT, Nguyen TB, Chen CW, Hung CM, Chang JH,
 Dong CD. Influence of pyrolysis temperature on polycyclic
 aromatic hydrocarbons production and tetracycline adsorption
 behavior of biochar derived from spent coffee ground.
 Bioresour Technol. 2019;284:197–203.
- [35] Wei FH, Zhang H, Ren QH, Chen HL, Yang LL, Ding B, et al. Removal of organic contaminants from wastewater with GO/ MOFs composites. PLoS One. 2021;16(7):e0253500.
- [36] Chen JF, Yang Y, Zhao SH, Bi FK, Song L, Liu N, et al. Stable black phosphorus encapsulation in porous mesh-like UiO-66 promoted charge transfer for photocatalytic oxidation of toluene and o-dichlorobenzene: Performance, degradation pathway, and mechanism. ACS Catal. 2022;12:8069-81.
- [37] Wei FH, Ren QH, Liang Z, Chen D. Synthesis of graphene oxide/ metal-organic frameworks composite materials for removal of Congo red from wastewater. Chemistryselect. 2019;4(19):5755-62.
- [38] Zhang XD, Bi FK, Zhao ZY, Yang Y, Li YT, Song L, et al. Boosting toluene oxidation by the regulation of Pd species on UiO-66: Synergistic effect of Pd species. J Catal. 2022;413:59–73.
- [39] Du QX, Rao RZ, Bi FK, Yang Y, Zhang WM, Yang YQ, et al. Preparation of modified zirconium-based metal-organic frameworks (Zr-MOFs) supported metals and recent application in environment: A review and perspectives. Surf Interfaces. 2022;28:101647.
- [40] Hu J, Yu H, Dai W, Yan X, Hu X, Huang H. Enhanced adsorptive removal ofhazardous anionic dye "Congo red" by a Ni/Cu mixed-component metal-organic porous material. RSC Adv. 2014:4:35124
- [41] Yılmaz E, Sert E, Atalay FS. Synthesis, characterization of a metal organic framework:MIL-53 (Fe) and adsorption mechanisms of methyl red onto MIL-53 (Fe). J Taiwan Inst Chem Eng. 2016;65:323–30.

- [42] Rostamian R, Behnejad H. Insights into doxycycline adsorption onto grapheme nanosheet: a combined quantum mechanics, thermodynamics, and kinetic study. Env Sci Pollut Res. 2018;25:2528–37.
- [43] Liu S, Xu WH, Liu YG, Tan XF, Zeng GM, Li X, et al. Facile synthesis of Cu(II) impregnated biochar with enhanced adsorption activity for the removal of doxycycline hydrochloride from water. Sci Total Env. 2017;592;546-53.
- [44] Ghaemi M, Absalan G. Fast removal and determination of doxycycline in water samples and honey by Fe3O4 magnetic nanoparticles. J Iran Chem Soc. 2015;12:1–7.
- [45] Zaidi S, Sivasankar V, Chaabane T, Alonzo V, Omine K, Maachi R, et al. Separate and simultaneous removal of doxycycline and oxytetracycline antibiotics by electrogenerated adsorbents (EGAs). J Env Chem Eng. 2019;7:102876.
- [46] Rego RM, Kurkuri MD, Kigga MA. Comprehensive review on water remediation using UiO-66 MOFs and their derivatives. Chemosphere. 2022;302:134845.
- [47] Chen J, Ouyang JB, Chen WQ, Zheng ZP, Yang Z, Liu ZR, et al. Fabrication and adsorption mechanism of chitosan/Zr-MOF (UiO-66) composite foams for efficient removal of ketoprofen from aqueous solution. Chem Eng J. 2022;431:134045.
- [48] Sriram G, Bendre A, Mariappan E, Altalhi T, Kigga M, Ching YC, et al. Recent trends in the application of metal-organic frameworks (MOFs) for the removal of toxic dyes and their removal mechanism-a review. Sustain Mater Techno. 2022;31:e00378.
- [49] Du CY, Zhang Y, Zhang Z, Zhou L, Yu GL, Wen XF, et al. Fe-based metal organic frameworks (Fe-MOFs) for organic pollutants removal via photo-Fenton: A review. Chem Eng J. 2022;431:133932.
- [50] Song FJ, Cao SR, Liu ZH, Su HT, Chen ZQ. Different decorated ZIF-67 adsorption performance towards methamphetamine revealed by theoretical and experimental investigations. J Mol Liq. 2022;364:119950.